ISSN 0021-3640, JETP Letters, 2023, Vol. 117, No. 9, pp. 708–715. © The Author(s), 2023. This article is an open access publication.
Russian Text © The Author(s), 2023, published in Pis'ma v Zhurnal Eksperimental'noi i Teoreticheskoi Fiziki, 2023, Vol. 117, No. 9, pp. 704–711.

CONDENSED MATTER

Excitonic Order in Strongly Correlated Systems with the Spin Crossover

Yu. S. Orlov[a, b, *], S. V. Nikolaev[a, b], and S. G. Ovchinnikov[a, b]

[a] *Siberian Federal University, Krasnoyarsk, 660041 Russia*

[b] *Kirensky Institute of Physics, Federal Research Center KSC, Siberian Branch, Russian Academy of Sciences, Krasnoyarsk, 660036 Russia*

**e-mail: jso.krasn@mail.ru*

Received March 22, 2023; revised March 31, 2023; accepted April 4, 2023

Features of the formation of the magnetic structure and the exciton Bose–Einstein condensate phase of magnetic excitons in strongly correlated systems near the spin crossover have been considered with the effective Hamiltonian obtained from the two-band Hubbard–Kanamori model. The coexistence of antiferromagnetism and exciton condensate, as well as the appearance of the long-range excitonic antiferromagnetic order even in the absence of the interatomic exchange interaction, has been revealed. The role of the electron–phonon coupling has been considered.

DOI: 10.1134/S0021364023600878

1. INTRODUCTION

Exciton condensation and excitonic insulator state have long been studied beginning with theoretical works [1–3]. Keldysh and Kopaev [3] showed that the modified Bardeen–Cooper–Schrieffer theory of superconductivity can be efficiently used to describe metal–insulator phase transitions in semimetals. A phase transition in a model appears at an arbitrarily weak electron–electron interaction and, by analogy with the superconducting phase transition, can be interpreted as the Bose–Einstein condensation of loosely bound electron–hole pairs (excitons with a large radius). The Keldysh–Kopaev model of excitonic insulators becomes a standard scheme of the description of electron–electron correlations in the weak interaction limit. Conditions for the formation of the excitonic ferromagnetism phase [4] in semimetals were determined within this model. The condensation of excitons in strongly correlated systems was actively discussed later (see, e.g., [5–13]). A new line of research is currently developed in excitonic magnetism associated with relatively close energies of the singlet and excited triplet ion states in Mott–Hubbard insulators [14] (some recent interesting results on excitonic magnetism can be found, e.g., in [15–17]). In this work, we consider features of the formation of the exciton condensate, which is a condensate of local (at a site of a crystal lattice) magnetic excitons (excitons with a small radius) in strongly correlated systems near spin crossover. The results obtained in this work are obtained using the Hubbard X operator formalism for the two-band Hubbard–Kanamori model. The appearance of a long-range antiferromagnetic order because of excitonic ordering even in the absence of the interatomic exchange interaction is revealed. The role of the electron–phonon coupling is examined. It is shown that the off-diagonal electron–phonon coupling, unlike the diagonal one, changes the symmetry of the excitonic order parameter and leads to its competition with antiferromagnetism.

2. EFFECTIVE HAMILTONIAN

The Hamiltonian of the two-band Hubbard–Kanamori model, which is the minimal model of strongly correlated systems with spin crossover, can be represented in the form

$$\hat{H} = \hat{H}_\Delta + \hat{H}_t + \hat{H}_{\text{Coulomb}}. \quad (1)$$

Here,

$$\hat{H}_\Delta = \varepsilon_1 \sum_{i,\gamma} c^\dagger_{1i\gamma} c_{1i\gamma} + \varepsilon_2 \sum_{i,\gamma} c^\dagger_{2i\gamma} c_{2i\gamma} \quad (2)$$

includes the single-ion energy of electrons in single-particle states with energy levels ε_1 and $\varepsilon_2 = \varepsilon_1 + \Delta$, where Δ is the energy of electrons in the crystal field ($\varepsilon_1 = 0$ can be set for convenience), i enumerates the sites of the lattice, and $\gamma = \pm 1/2$ is the projection of the electron spin. The second term in Eq. (1) is given by the expression

$$\begin{aligned}\hat{H}_t = {} & t_{11} \sum_{\langle i,j\rangle,\gamma} c^\dagger_{1i\gamma} c_{1j\gamma} + t_{22} \sum_{\langle i,j\rangle,\gamma} c^\dagger_{2i\gamma} c_{2j\gamma} \\ & + t_{12} \sum_{\langle i,j\rangle,\gamma} \left(c^\dagger_{2i\gamma} c_{1j\gamma} + c^\dagger_{1i\gamma} c_{2j\gamma} \right),\end{aligned} \quad (3)$$

where $t_{\lambda\lambda'}$ are the hopping parameters ($\lambda,\lambda' = 1,2$ are the orbital indices) describing hop of electrons between the nearest neighbor sites of the crystal lattice with the energy levels ε_1 and ε_2. The third term in Eq. (1) has the form

$$\begin{aligned}\hat{H}_{\text{Coulomb}} &= U\sum_{\lambda,i} c^{\dagger}_{\lambda i\uparrow}c^{\dagger}_{\lambda i\downarrow}c_{\lambda i\uparrow}c_{\lambda i\downarrow} \\ &+ V\sum_{\lambda\neq\lambda',i} c^{\dagger}_{\lambda i\uparrow}c^{\dagger}_{\lambda' i\downarrow}c_{\lambda i\uparrow}c_{\lambda' i\downarrow} \\ &+ V\sum_{\lambda>\lambda',i,\gamma} c^{\dagger}_{\lambda i\gamma}c^{\dagger}_{\lambda' i\gamma}c_{\lambda i\gamma}c_{\lambda' i\gamma} \\ &+ J_{\text{H}}\sum_{\lambda>\lambda',i,\gamma} c^{\dagger}_{\lambda i\gamma}c^{\dagger}_{\lambda' i\gamma}c_{\lambda' i\gamma}c_{\lambda i\gamma} \\ &+ J_{\text{H}}\sum_{\lambda\neq\lambda',i} c^{\dagger}_{\lambda i\uparrow}c^{\dagger}_{\lambda' i\downarrow}c_{\lambda' i\uparrow}c_{\lambda i\downarrow} \\ &+ J'_{\text{H}}\sum_{\lambda\neq\lambda',i} c^{\dagger}_{\lambda i\uparrow}c^{\dagger}_{\lambda i\downarrow}c_{\lambda' i\uparrow}c_{\lambda' i\downarrow}\end{aligned} \tag{4}$$

and contains the single-site energy of the Coulomb interaction between electrons (the electron–electron interaction is considered in the Kanamori approximation with diagonal, U, and off-diagonal, V, matrix elements in orbital indices and with the Hund exchange interaction parameters J_{H} and J'_{H} [18]).

An important feature of such two-orbital model is that various localized multielectron (two-particle) states (terms), which are characterized by the spins $S = 0,1$, and the crossover between them with increasing Δ can appear in the case of the half filling (the average number of electrons per site of the crystal lattice is $N_e = 2$) and in the zeroth approximation in the intersite hopping parameters $t_{\lambda\lambda'} = 0$. In the region $\Delta < \Delta_C = \sqrt{(U - V + J_{\text{H}})^2 + J'^2_{\text{H}}}$, the ground state is the triplet ($S = 1$) HS state $|\sigma\rangle$ with the energy E_{HS}, which is triply degenerate in spin projection $\sigma = 0,\pm1$:

$$|\sigma\rangle = \begin{cases} a^{\dagger}_{1\uparrow}a^{\dagger}_{2\uparrow}|0\rangle, & \sigma = +1 \\ \dfrac{1}{\sqrt{2}}\left(a^{\dagger}_{1\uparrow}a^{\dagger}_{2\downarrow}|0\rangle + a^{\dagger}_{1\downarrow}a^{\dagger}_{2\uparrow}|0\rangle\right), & \sigma = 0, \\ a^{\dagger}_{1\downarrow}a^{\dagger}_{2\downarrow}|0\rangle, & \sigma = -1 \end{cases}$$

At $\Delta > \Delta_C$, the ground state is the singlet ($S = 0$) LS state $|s\rangle = C_1(\Delta)a^{\dagger}_{1\uparrow}a^{\dagger}_{1\downarrow}|0\rangle - C_2(\Delta)a^{\dagger}_{2\uparrow}a^{\dagger}_{2\downarrow}|0\rangle$ with the energy E_{LS}, where $C_1(\Delta) = \sqrt{1 - C_2^2(\Delta)}$ and $C_2(\Delta) = x/2\left(1 + x + \sqrt{1+x}\right)$ are the normalization coefficients ($x = J'^2_{\text{H}}/\Delta^2$).

To derive the effective Hamiltonian, it is convenient to use the Hubbard X operators $X^{p,q} = |p\rangle\langle q|$ [19], which are expressed in terms of the eigenstate of the Hamiltonian $\hat{H}_{\Delta} + \hat{H}_{\text{Coulomb}}$

$$\left(\hat{H}_{\Delta} + \hat{H}_{\text{Coulomb}}\right)|p\rangle = E_p|p\rangle \tag{5}$$

with the numbers of electrons $N_e = 0,1,2,3,4$. Since the Hubbard operators form a linearly independent basis, any local operator can be expressed in terms of a linear combination of the X operators. In particular, the single-electron annihilation (creation) operator is represented in the form

$$c_{\lambda i\gamma} = \sum_{pq}|p\rangle\langle p|c_{\lambda i\gamma}|q\rangle\langle q| = \sum_{pq}\chi_{\lambda\gamma}(p,q)X_i^{p,q}. \tag{6}$$

Since the number of different root vectors (p,q) introduced by Zaitsev [20] is finite, they can be enumerated, and the number m of the mth vector has the meaning of the band index of local Fermi quasiparticles. Then, $c_{i\lambda\gamma} = \sum_m \chi_{\lambda\gamma}(m)X_i^m$, $c^{\dagger}_{i\lambda\gamma} = \sum_m \chi^*_{\lambda\gamma}(m)X_i^{m\dagger}$. Using Eq. (6), the anomalous averages $\left\langle a^{\dagger}_{2f\gamma}a_{1f\gamma}\right\rangle$ (without spin flip) and $\left\langle a^{\dagger}_{2f\bar{\gamma}}a_{1f\gamma}\right\rangle$ (with spin flip, $\bar{\gamma} = -\gamma$) can be represented in the form

$$\left\langle c^{\dagger}_{2f\gamma}c_{1f\gamma}\right\rangle \approx -\gamma\sqrt{2}\left(C_2\left\langle X_f^{s,0}\right\rangle + C_1\left\langle X_f^{0,s}\right\rangle\right), \tag{7}$$

$$\begin{aligned}\left\langle c^{\dagger}_{2f\bar{\gamma}}c_{1f\gamma}\right\rangle \approx{}& 2\gamma\left(\gamma - \frac{1}{2}\right)\left(C_2\left\langle X_f^{s,-1}\right\rangle + C_1\left\langle X_f^{-1,s}\right\rangle\right) \\ &- 2\gamma\left(\gamma + \frac{1}{2}\right)\left(C_2\left\langle X_f^{s,+1}\right\rangle + C_1\left\langle X_f^{+1,s}\right\rangle\right).\end{aligned} \tag{8}$$

Here, the angle brackets $\langle\ldots\rangle$ stand for a thermodynamic mean and the means of the X operators built on one- and three-electron states are omitted because their contribution is negligibly small in the considered case of half filling (two-particle states) with a fixed number of electrons per site of the crystal lattice (the homopolar model of solid).

As seen in Eqs. (7) and (8), excitonic pairing is described by nonzero means of singlet excitations. The Hamiltonian (1) in the representation of Hubbard X operators has the form

$$\hat{H} = \sum_{i,p}E_pX_i^{p,p} + \sum_{\langle i,j\rangle}\sum_{mn}t^{mn}X_i^{m\dagger}X_j^n. \tag{9}$$

Here, E_p is the energy of multielectron terms and $t^{mn} = \sum_{\lambda,\lambda',\gamma}t_{\lambda\lambda'}\chi^*_{\lambda\gamma}(m)\chi_{\lambda'\gamma}(n)$ are the renormalized hopping parameters.

Using the projection operator method developed in [21] for the Hubbard model and in [22] for the p–d model (see also [5, 6]) to exclude interband hops from the Hamiltonian (9), we can obtain the effective Hamiltonian in the form

$$\hat{H}_{\text{eff}} = \hat{H}_S + \hat{H}_{n_{\text{LS}}n_{\text{LS}}} + \hat{H}_{ex}. \tag{10}$$

Here, the first term is the Heisenberg Hamiltonian containing the interatomic exchange interaction

$$\hat{H}_S = \frac{1}{2}J\sum_{\langle i,j\rangle}\left(S_iS_j - \frac{1}{4}\hat{n}_i\hat{n}_j\right), \quad (11)$$

where $\hat{\mathbf{S}}_i$ is the spin-1 operator, which can be specified by the components $\hat{S}_i^+ = \sqrt{2}\left(X_i^{+1,0} + X_i^{0,-1}\right)$, $\hat{S}_i^- = \sqrt{2}\left(X_i^{0,+1} + X_i^{-1,0}\right)$, and $\hat{S}_i^z = X_i^{+1,+1} - X_i^{-1,-1}$ [23]; $J = \left(t_{11}^2 + 2t_{12}^2 + t_{22}^2\right)/\Omega_g$ is the magnitude of the interatomic exchange interaction; Ω_g is the energy of charge transfer between the centers of the upper and lower Hubbard subbands [21, 22]; and $\hat{n}_i = 2\left(X_i^{s,s} + \sum_\sigma X_i^{\sigma,\sigma}\right) = 2\left(\hat{n}_i^{\mathrm{LS}} + \hat{n}_i^{\mathrm{HS}}\right)$ is the operator of the number of particles at the ith site ($\hat{n}_i^{\mathrm{LS(HS)}}$ is the occupation number operator of the LS (HS) state). Using the condition of completeness $X^{s,s} + \sum_\sigma X^{\sigma,\sigma} = 1$, one can show that $\langle\hat{n}_i\rangle = 2\left(\left\langle\hat{n}_i^{\mathrm{LS}}\right\rangle + \left\langle\hat{n}_i^{\mathrm{HS}}\right\rangle\right) = 2\left(n_{\mathrm{LS}} + n_{\mathrm{HS}}\right) = 2$, where $n_{\mathrm{LS(HS)}}$ is the average number of particles in the LS (HS) state ($n_{\mathrm{LS}} + n_{\mathrm{HS}} = 1$).

The second term in Eq. (10) is given by the formula

$$\hat{H}_{n_{\mathrm{LS}}n_{\mathrm{LS}}} = \frac{1}{2}\tilde{J}\sum_{\langle i,j\rangle}X_i^{s,s}X_j^{s,s}, \quad (12)$$

where $\tilde{J} = \left[1 - \left(2C_1C_2\right)^2\right]\left(t_{11}^2 - 2t_{12}^2 + t_{22}^2\right)/\Omega_g$, and describes the density–density interaction between low-spin states.

The third term in Eq. (10) has the form

$$\hat{H}_{ex} = -\frac{\varepsilon_S}{2}\sum_i\left(X_i^{s,s} - \sum_{\sigma=-S}^{+S}X_i^{\sigma,\sigma}\right) + \sum_\sigma\sum_{\langle i,j\rangle}\left[\frac{1}{2}J_{ex}^{'}\left(X_i^{\sigma,s}X_j^{s,\sigma} + X_i^{s,\sigma}X_j^{\sigma,s}\right) - \frac{1}{2}J_{ex}^{''}(-1)^{|\sigma|}\left(X_i^{\sigma,s}X_j^{\bar{\sigma},s} + X_i^{s,\sigma}X_j^{s,\bar{\sigma}}\right)\right], \quad (13)$$

where $\varepsilon_S = E_{\mathrm{HS}} - E_{\mathrm{LS}}$ is the spin gap and $\bar{\sigma} = -\sigma$, and includes interatomic hops of excitons with the amplitude $J_{ex}^{'} = 2C_1C_2\left(t_{11}t_{22} - t_{12}^2\right)/\Omega_g$ and the creation/annihilation of biexcitons at neighboring sites with the amplitude $J_{ex}^{''} = \left(t_{11}t_{22} - t_{12}^2\right)/\Omega_g$ taking into account the energy of electronic configurations of the LS and HS states. In the absence of cooperative interactions, the ground state in the cases of negative and positive spin gap is the HS and LS states, respectively. The Hubbard operators $X_i^{\sigma,s}$ and $X_i^{s,\sigma}$ in Eq. (13) describe Bose excitations (excitons) at the ith site from the low-spin singlet state $|s\rangle$ to the high-spin triplet one $|\sigma\rangle$ with the spin projection $\sigma = 0, \pm1$ and back, respectively. The first term in square brackets in Eq. (13) describes the dispersion of excitons caused by interatomic hops; this dispersion was considered in [24]. The second term in square brackets in Eq. (13) involves the creation and annihilation of biexciton at the neighboring ith and jth sites of the lattice, which complicates the dispersion of excitons compared to the conventional dispersion in the tight binding method [24]. Near the spin crossover, $C_1 \approx 1$ and $C_2 \approx 0$; consequently, $J_{ex}^{'} \approx 0$. Under these conditions, biexcitons make the main contribution to the formation of dispersion of excitons. The Hamiltonian (13) describes the kinetic exciton–exciton interaction [25] in the representation of Hubbard X operators.

The expression in square brackets in Eq. (13) can be represented in the form

$$\frac{1}{2}J_{ex}^{'}\sum_{\langle i,j\rangle}\left(\hat{\mathbf{d}}_i^\dagger\cdot\hat{\mathbf{d}}_j + \hat{\mathbf{d}}_i\cdot\hat{\mathbf{d}}_j^\dagger\right) - \frac{1}{2}J_{ex}^{''}\sum_{\langle i,j\rangle}\left(\hat{\mathbf{d}}_i^\dagger\cdot\hat{\mathbf{d}}_j^\dagger + \hat{\mathbf{d}}_i\cdot\hat{\mathbf{d}}_j\right). \quad (14)$$

Here, $\hat{d}_x = \frac{1}{\sqrt{2}}\left(-\hat{d}_+ + \hat{d}_-\right)$, $\hat{d}_y = \frac{1}{\sqrt{2}i}\left(\hat{d}_+ + \hat{d}_-\right)$, and $\hat{d}_z = \hat{d}_0$ [11], where $\hat{d}_+ = X^{s,+}$, $\hat{d}_- = X^{s,-}$, and $\hat{d}_0 = X^{s,0}$. The vector $\hat{\mathbf{d}} = \left(\hat{d}_x, \hat{d}_y, \hat{d}_z\right)$ corresponds to the so-called **d** vector in the triplet superconductivity theory.

3. PHASE DIAGRAMS IN THE MEAN FIELD APPROXIMATION

In the mean field (MF) approximation for two sublattices A and B, Eq. (11) becomes

$$\hat{H}_S^{\mathrm{MF}} = zJm_B\sum_{i_A}\hat{S}_{i_A}^z + zJm_A\sum_{i_B}\hat{S}_{i_B}^z - zJ\frac{1}{4}n_B\sum_{i_A}\hat{n}_{i_A} - zJ\frac{1}{4}n_A\sum_{i_B}\hat{n}_{i_B} - \frac{1}{2}zJNm_Am_B + \frac{1}{2}zJN, \quad (15)$$

where z is the number of the nearest neighbors and $m_{A(B)} = \left\langle\hat{S}_{i_{A(B)}}^z\right\rangle$ is the magnetization of the sublattice $A(B)$; Eq. (12) takes the form

$$\hat{H}_{n_{\mathrm{LS}}n_{\mathrm{LS}}}^{\mathrm{MF}} = z\tilde{J}n_{\mathrm{LS},B}\sum_{i_A}\hat{n}_{i_A}^{\mathrm{LS}} + z\tilde{J}n_{\mathrm{LS},A}\sum_{i_B}\hat{n}_{i_B}^{\mathrm{LS}} - z\tilde{J}\frac{N}{2}n_{\mathrm{LS},A}n_{\mathrm{LS},B}, \quad (16)$$

where the interaction $\tilde{J}$ leads to an additional cooperativity mechanism and stabilizes the HS state; and Eq. (13) is modified to the form

$$\hat{H}_{ex}^{\mathrm{MF}} = \sum_{F}\sum_{\sigma=\pm1,0}\left\{zJ'_{ex}\Delta^{\sigma}_{ex,\bar{F}}\sum_{i_F}\left(X^{s,\sigma}_{i_F}+X^{\sigma,s}_{i_F}\right)\right.$$
$$-(-1)^{|\sigma|}zJ''_{ex}\Delta^{\sigma}_{ex,\bar{F}}\sum_{i_F}\left(X^{s,\bar{\sigma}}_{i_F}+X^{\bar{\sigma},s}_{i_F}\right)$$
$$\left.-\frac{1}{2}zN\left(J'_{ex}\Delta^{\sigma}_{ex,F}\Delta^{\sigma}_{ex,\bar{F}}-(-1)^{|\sigma|}J''_{ex}\Delta^{\sigma}_{ex,F}\Delta^{\bar{\sigma}}_{ex,\bar{F}}\right)\right\} \quad (17)$$
$$-\varepsilon_S\sum_{i_A}X^{s,s}_{i_A}-\varepsilon_S\sum_{i_B}X^{s,s}_{i_B}+N\frac{\varepsilon_S}{2},$$

where $F = A, B$ ($\bar{F} = A$ and B if $F = B$ and A, respectively, and $\Delta^{\sigma}_{ex,A(B)} = \left\langle X^{s,\sigma}_{i_A(i_B)}\right\rangle$ are the components of the excitonic order parameter, which satisfy the equality $\left(\Delta^{\sigma}_{ex}\right)^{\dagger} = \left\langle X^{\sigma,s}\right\rangle = \Delta^{\sigma}_{ex}$ in the thermodynamically equilibrium state. Unlike zero mean values, $\Delta^{\sigma}_{ex} \neq 0$ means the quantum-mechanical mixing of the LS and HS states but in the absence of the spin–orbit coupling.

Using the solutions of the eigenvalue problem

$$\hat{H}^{\mathrm{MF}}_{\mathrm{eff}}\left|\psi_k\right\rangle = E_k\left|\psi_k\right\rangle, \quad (18)$$

where $\left|\psi_k\right\rangle = C_{LS,k}\left|s\right\rangle + \sum_{\sigma}C_{\mathrm{HS},k,\sigma}\left|\sigma\right\rangle$ are the eigenstates of the Hamiltonian $\hat{H}^{\mathrm{MF}}_{\mathrm{eff}} = \hat{H}^{\mathrm{MF}}_{S} + \hat{H}^{\mathrm{MF}}_{nn} + \hat{H}^{\mathrm{MF}}_{ex}$, that correspond to the minimum of the free energy $F = -k_{\mathrm{B}}T\ln Z$, where $Z = \sum_k e^{-E_k/k_{\mathrm{B}}T}$ is the partition function of the system, one can calculate various thermodynamic averages appearing in $\hat{H}^{\mathrm{MF}}_{\mathrm{eff}}$:

$$\Delta^{\sigma}_{ex,A(B)} = \frac{1}{Z}\sum_k\left\langle\psi_k\left|X^{s,\sigma}_{i_{A(B)}}\right|\psi_k\right\rangle e^{-E_k/k_{\mathrm{B}}T},$$

$$m_{A(B)} = \frac{1}{Z}\sum_k\left\langle\psi_k\left|S^{z}_{i_{A(B)}}\right|\psi_k\right\rangle e^{-E_k/k_{\mathrm{B}}T},$$

$$n_{\mathrm{HS},A(B)} = \frac{1}{Z}\sum_k\left\langle\psi_k\left|\sum_{\sigma}X^{\sigma,\sigma}_{i_{A(B)}}\right|\psi_k\right\rangle e^{-E_k/k_{\mathrm{B}}T}.$$

Equation (18) specifies a self-consistent problem of determining the eigenstates and eigenvalues of the effective Hamiltonian in the mean field approximation.

Figure 1 shows the (T, ε_S) phase diagrams of (a, b) the population of the HS state n_{HS}, (c, d) the magnetization m, and (e, f) the components of the excitonic order parameter $\Delta^{+/-}$ for two sublattices A and B with calculated the parameters at $J = J_0 = 28$ K [26]. The results near the crossover on a magnified scale are given in the right panels. Here, the temperature T and the spin gap ε_S are given in units of the Néel temperature $T_{\mathrm{N}} = zJ_0S(S+1)/3$ ($S = 1$) and the exchange integral J_0, respectively. The long-range antiferromagnetic order occurs in the system (see Figs. 1c, 1d), and $m_A = -m_B$. It is seen that the antiferromagnetic HS ground state AFM(HS) holds up to $\varepsilon_S = \varepsilon_S^{c_2} \approx 4J_0$ because of the cooperative exchange interaction J in the system (see Figs. 1c, 1d), although the ground state in the single-ion picture at $\varepsilon_S > \varepsilon_S^{c} = 0$ is the LS state. Cooperative effects obviously increase the critical spin gap ε_S^{c} because the exchange interaction J and the interaction $\tilde{J}$ stabilize the HS state, reducing its energy. The antiferromagnetic HS ground state changes at $\varepsilon_S > \varepsilon_S^{c_2}$ to the diamagnetic LS state, DM(LS) (see Figs. 1c, 1d).

The diagram in Fig. 1b demonstrates the tricritical point (ε_S^{*}, T^{*}), where the line of a second-order phase transition is continuously transformed to the line of a first-order phase transition, and the bicritical point (ε_S^{**}, T^{**}), where the line of the first-order phase transition is separated into two lines of the second-order phase transition according to the Gibbs phase rule.

The exciton condensate region appears at $\varepsilon_S^{c_1} < \varepsilon_S < \varepsilon_S^{c_2}$ (see Fig. 1f) and coexists with the long-range antiferromagnetic order (see Fig. 1d). Furthermore, the formation of the exciton condensate promotes antiferromagnetic ordering and the appearance of the magnetization in the region $\varepsilon_S^{c_0} < \varepsilon_S < \varepsilon_S^{c_2}$, where the long-range magnetic order is absent at $J''_{ex} = 0$. The black solid and dashed lines in Fig. 1d are the lines of the second- and first-order phase transitions at $J''_{ex} = 0$, respectively. In this case, the AFM(HS) ground state holds up to $\varepsilon_S = \varepsilon_S^{c_0} \approx 3J_0 < \varepsilon_S^{c_2}$, and the phase diagram demonstrates only one tricritical point marked by a triangle (see Fig. 1d).

A nonzero population of the HS state (see Figs. 1a, 1b) and the magnetization (see Figs. 1c, 1d) appear at $\varepsilon_S^{c_0} < \varepsilon_S < \varepsilon_S^{c_2}$ because of the formation of the exciton condensate (see Figs. 1e, 1f). This is physically explained by the structure of the excitonic order parameter. This structure at $J > 0$ and $J''_{ex} > 0$ is such that $\Delta^{+}_{A} = 0$, $\Delta^{-}_{A} = -\Delta^{+}_{B}$, and $\Delta^{-}_{B} = 0$ if $\Delta^{-}_{A} \neq 0$, and $\Delta^{-}_{A} = 0$, $\Delta^{-}_{B} = -\Delta^{+}_{A}$, and $\Delta^{+}_{B} = 0$ if $\Delta^{+}_{A} \neq 0$. The parameters Δ^{0}_{A} and Δ^{0}_{B} are zero. Nonzero corresponding averages $\Delta^{+/-}$ on different sublattices promote the formation of antiferromagnetism and allow its coexistence with the exciton condensate.

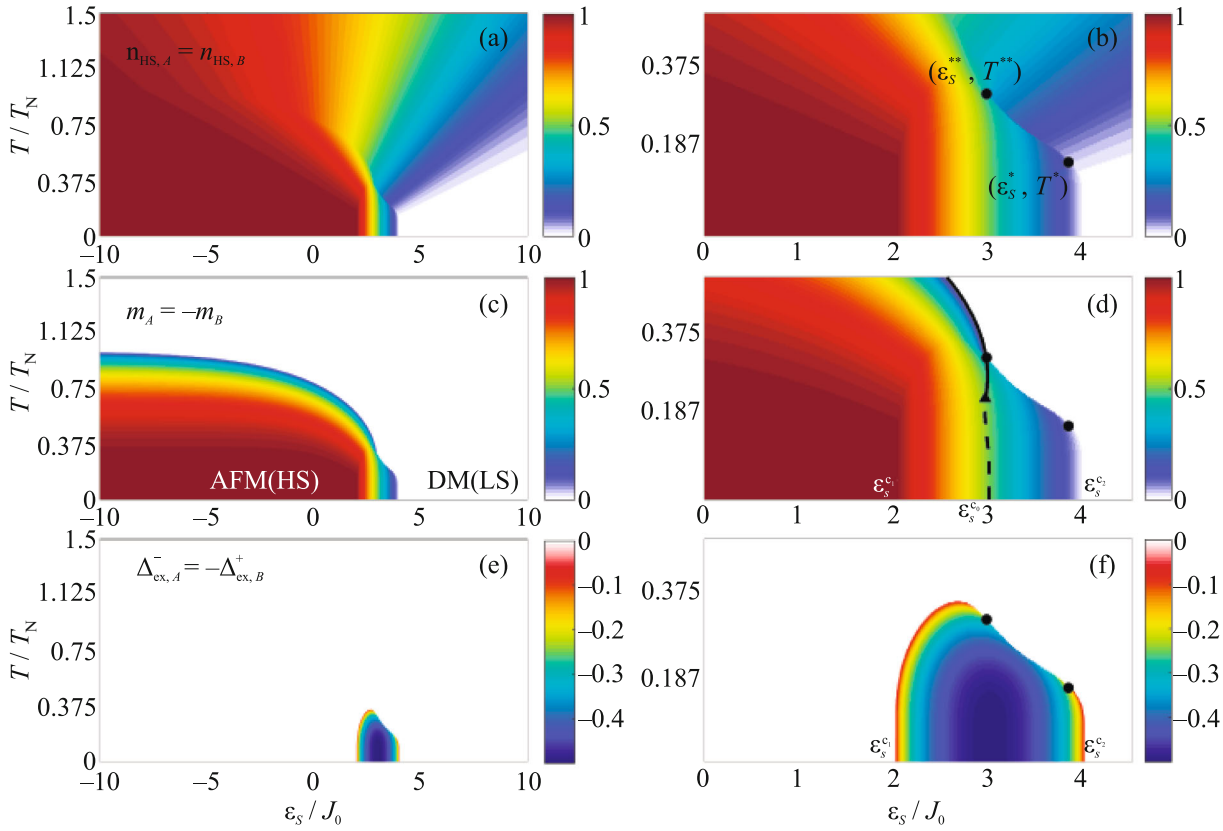

Fig. 1. (Color online) Phase diagrams of (a, b) the population of the HS state n_{HS}, (c, d) the magnetization m, and (e, f) the components of the excitonic order parameter Δ^{σ}_{ex} for two sublattices A and B calculated with the parameters $z = 4$, $J = J_0$, $\tilde{J} = 0.5J_0$, and $J^{''}_{ex} = 0.5J_0$. The results near the crossover on a magnified scale are given in panels (b, d, f).

According to the aforesaid, the case with $J = 0$ and $J^{''}_{ex} \neq 0$ is of interest. Figure 2 shows the (T, ε_S) phase diagrams of the components of the excitonic order parameter Δ^{σ}_{ex}, the population of the HS state n_{HS}, and the magnetization m for two sublattices A and B. The calculations involved the interatomic exchange interaction at $J = 0$, but the temperature T and the spin gap ε_S here and below are also given in units of the Néel temperature T_N and the exchange integral J_0, respectively, for convenient comparison with the case $J \neq 0$ considered above. It is seen that $n_{HS,A} = n_{HS,B}$ (see Fig. 2d); $m_A = -m_B$; i.e., the long-range antiferromagnetic order exists in the system (see Fig. 2e) even at $J = 0$ because $\Delta^{+}_{ex,A(B)} \neq \Delta^{-}_{ex,A(B)}$ (see Figs. 2a, 2b), whereas $\Delta^{0}_{ex,A} = \Delta^{0}_{ex,B}$ (see Fig. 2c), and $\Delta^{+/-}_{ex,A}$ and $\Delta^{+/-}_{ex,B}$ are opposite in sign and are equal in absolute value (see Figs. 2a, 2b).

The phase diagrams (see Fig. 2) clearly demonstrate the tricritical point $(\varepsilon^{*}_S, T^{*})$, where the line of second-order phase transitions is continuously transformed to the line of a first-order phase transitions. An increase in the temperature is accompanied by a second-order phase transition of the system from the AFM(HS) state to the paramagnetic state in the region $\varepsilon_S > \varepsilon^{*}_S$ (see Fig. 2e) and by a first-order phase transition in the region $\varepsilon_S < \varepsilon^{*}_S$. The asymmetry of all phase diagrams (see Fig. 2) with respect to the change in the sign of the spin gap is due to different orders of degeneracy of the HS and LS states.

To conclude this section, we discuss our results in comparison with the results on "excitonic ferromagnetism" obtained in [4], where the electron–phonon coupling is considered in addition to the electron–electron interaction and the corresponding situation can be briefly described as follows. The magnetic structure of a spin density wave type occurs as known in metals, where the topology of the multiconnected Fermi surface is characterized by the existence of the electron and hole regions superimposed at the parallel translation at a certain vector $\mathbf{q}$. The spin density wave is due to the triplet pairing of single-particle excitations of superimposed electron and hole regions of the Fermi surface. The picture is complicated if the spin density wave is imposed on a charge density wave

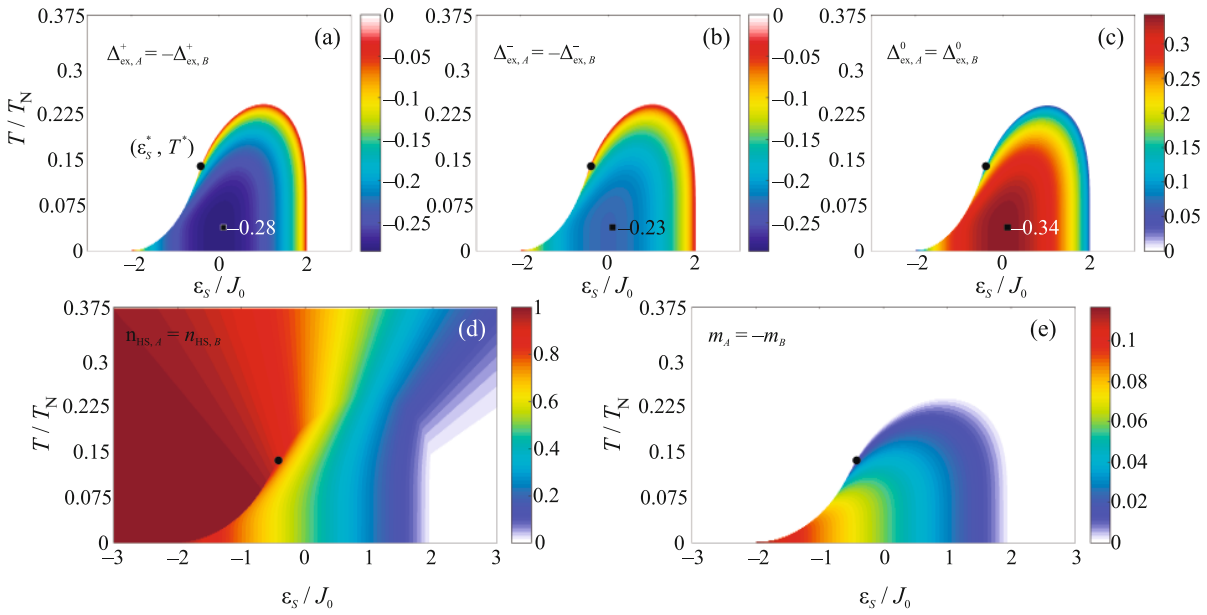

Fig. 2. (Color online) Phase diagrams of (a–c) the components of the excitonic order parameter Δ^{σ}_{ex}, (d) the population of the HS state n_{HS}, and (e) the magnetization m for two sublattices A and B calculated with the parameters $z = 4$, $J = \tilde{J} = 0$, and $J''_{ex} = 0.5J_0$. At the point ($\varepsilon_S/J_0 = 0.1$, $T/T_{\mathrm{N}} = 0.04$) marked by the black square, $\Delta^{\sigma}_{ex,A}$ values are given.

existing in the system because of the singlet pairing of electron and hole states. Coexisting single-phase commensurate spin and charge density waves induce an additional magnetic splitting of the spectrum of single-particle excitations. As a result, the magnetic moment of the unit volume of the crystal appears under doping; this is the so-called excitonic ferromagnetism. By analogy with [4], the appearance of the long-range antiferromagnetic order caused by the formation of the exciton phase can be called "excitonic antiferromagnetism."

4. ROLE OF THE ELECTRON–PHONON COUPLING

As seen, the structure and symmetry of the excitonic order parameter determine the possibility of the appearance of antiferromagnetism and its coexistence with the exciton condensate (see Figs. 1, 2). In the absence of the interatomic exchange interaction, the magnetization is an improper order parameter because it is due to exciton ordering (see Fig. 2). The electron–phonon coupling is one of the factors that can change the structure (symmetry) of the excitonic order parameter. Taking into account the electron–phonon coupling, instead of Eq. (18), we have

$$\hat{H}\left|\psi_k\right\rangle = E_k\left|\psi_k\right\rangle, \tag{19}$$

where $\left|\psi_k\right\rangle$ are the eigenstates of the Hamiltonian $\hat{H} = \hat{H}^{\mathrm{MF}}_{\mathrm{eff}} + \hat{H}_{1ph} + \hat{H}_{2ph}$. Here,

$$\hat{H}_{1ph} = \omega_{0(1)}\sum_i\left(a_i^{\dagger}a_i + \frac{1}{2}\right) + g_1\sum_i\left(a_i + a_i^{\dagger}\right)\left(X_i^{s,s} - \sum_{\sigma=-1}^{+1}X_i^{\sigma,\sigma}\right) \tag{20}$$

includes the diagonal electron–phonon coupling, and

$$\hat{H}_{2ph} = \omega_{0(2)}\sum_i\sum_{\sigma=-1}^{+1}\left(b_{i,\sigma}^{\dagger}b_{i,\sigma} + \frac{1}{2}\right) + g_2\sum_i\sum_{\sigma=-1}^{+1}\left(b_{i,\sigma} + b_{i,\sigma}^{\dagger}\right)\left(X_i^{s,\sigma} + X_i^{\sigma,s}\right) \tag{21}$$

describes off-diagonal electron–phonon processes of the transition from the singlet $\left|s\right\rangle$ to triplet state $\left|\sigma\right\rangle$ and back. In Eqs. (20) and (21), g_1 and g_2 are the electron–phonon coupling constants and $\omega_{0(1)}$ and $\omega_{0(2)}$ are the frequencies of a- and b-type phonons, respectively.

The diagonal electron–phonon coupling (20) does not lead to qualitative changes. The symmetry of the excitonic order parameter does not change, but the region of the exciton condensate decreases with increasing g_1; i.e., the diagonal electron–phonon coupling suppresses the exciton condensate phase. On the contrary, the off-diagonal electron–phonon coupling (21) changes the symmetry of the excitonic

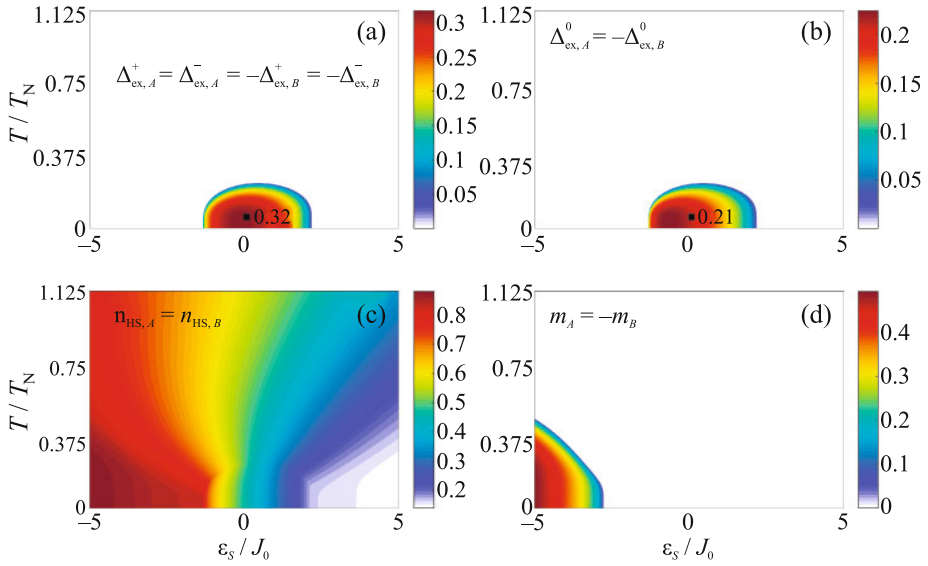

Fig. 3. (Color online) Phase diagrams of (a, b) the components of the excitonic order parameter Δ^{σ}_{ex}, (c) the population of the HS state n_{HS}, and (d) the magnetization m for two sublattices A and B calculated including the off-diagonal electron–phonon coupling and with the parameters $z = 4$, $J = J_0$, $\tilde{J} = 0.0$, $J''_{ex} = 0.6J_0$, $g_1 = 0.0$, and $g_2 = 5.8J_0$. At the point ($\varepsilon_S/J_0 = 0.08$, $T/T_N = 0.06$) marked by the black square, values $\Delta^{+}_{ex,A} = 0.32$ and $\Delta^{0}_{ex,A} = 0.21$ are given in panels (a) and (b), respectively.

order parameter. In this case, $\Delta^{\sigma}_{A} = -\Delta^{\sigma}_{B}$, $\Delta^{+}_{A(B)} = \Delta^{-}_{A(B)}$, and $\left|\Delta^{+/-}_{A(B)}\right| \neq \left|\Delta^{0}_{A(B)}\right|$, which excludes the coexistence of antiferromagnetism and exciton condensate. Figure 3 presents the phase diagrams calculated taking into account only the off-diagonal electron–phonon coupling (21). It is seen that the antiferromagnetism region decreases (see Fig. 3d) and differs from the exciton condensate region (see Figs. 3a, 3b). An increase in g_2 results in the expansion of the exciton condensate region and in the suppression of antiferromagnetism.

5. DISCUSSION AND CONCLUSIONS

Two cases can be separated using Eq. (1). In the first (weakly correlated) case, where $\hat{H}_{\text{Coulomb}} \lll \hat{H}_{\Delta} + \hat{H}_{t}$, we have a two-band semiconductor or a semimetal (depending on the relation between Δ and t), where the exciton condensate can be formed through the Bose–Einstein condensation or Bardeen–Cooper–Schrieffer scenario. In the second (strongly correlated) case, where the Coulomb energy of electrons becomes comparable with the energy of the crystal field $\hat{H}_{\text{Coulomb}} \sim \hat{H}_{\Delta}$ and higher than their kinetic energy $\hat{H}_{\text{Coulomb}} > \hat{H}_{t}$, the spin crossover becomes possible and localized magnetic excitons can be formed. In this work, we have shown within the two-band Hubbard model that the condensation of such excitons occurs near the spin crossover, which in turn results in the antiferromagnetic order even in the absence of the interatomic exchange interaction. We have detected the appearance of antiferromagnetism caused by the Bose–Einstein condensate of excitons. It is worth noting that the formation of the exciton condensate in the excitonic insulator model at a weak electron–electron interaction can also lead to the appearance of the magnetic order in the absence of the exchange interaction [4].

Studies of systems with the spin crossover, where the LS state is the ground state and the HS state is separated from it by the spin gap ε_S, in strong magnetic fields are of particular interest [27–31] because the critical magnetic field $B = B_c$ leads to the crossing of terms (magnetically induced spin crossover). One example is a new magnetic transition in $LaCoO_3$ recently detected in a strong magnetic field [28]; it can be attributed to the condensation of magnetic excitons [12, 13]. The model considered in this work and the results obtained can be used to explain the unconventional behavior of $LaCoO_3$ [28] and $(Pr_{1-y}Y_y)_{0.7}Ca_{0.3}CoO_3$ [32] in strong magnetic fields.

FUNDING

This work was supported jointly by the Russian Science Foundation and Krasnoyarsk Regional Science Foundation (project no. 22-22-20007).

CONFLICT OF INTEREST

The authors declare that they have no conflicts of interest.

OPEN ACCESS

REFERENCES

1. N. F. Mott, Philos. Mag. **6** (62), 287 (1961).
2. R. S. Knox, *The Theory of Excitons in Solid State Physics,* Ed. by F. Seitz and D. Turnbull (Academic, New York, 1963).
3. L. V. Keldysh and Y. V. Kopaev, Sov. Phys. Solid State **6**, 2219 (1965).
4. B. A. Volkov, Y. V. Kopaev, and A. I. Rusinov, Sov. Phys. JETP **41**, 952 (1975).
5. J. Kuneš, J. Phys.: Condens. Matter **27**, 333201 (2015).
6. J. Nasu, T. Watanabe, M. Naka, and S. Ishihara, Phys. Rev. B **93**, 205136 (2016).
7. P. Werner and A. J. Millis, Phys. Rev. Lett. **99**, 126405 (2007).
8. R. Suzuki, T. Watanabe, and S. Ishihara, Phys. Rev. B **80**, 054410 (2009).
9. L. Balents, Phys. Rev. B **62**, 2346 (2000).
10. T. Kaneko and Y. Ohta, Phys. Rev. B **90**, 245144 (2014).
11. J. Kuneš and P. Augustinský, Phys. Rev. B **89**, 115134 (2014).
12. A. Sotnikov and J. Kuneš, Sci. Rep. **6**, 30510 (2016).
13. T. Tatsuno, E. Mizoguchi, J. Nasu, M. Naka, and S. Ishihara, J. Phys. Soc. Jpn. **85**, 083706 (2016).
14. G. Khaliullin, Phys. Rev. Lett. **111**, 197201 (2013).
15. C. A. Belvin, E. Baldini, I. O. Ozel, D. Mao, H. C. Po, C. J. Allington, S. Son, B. H. Kim, J. Kim, I. Hwang, J. H. Kim, J.-G. Park, T. Senthil, and N. Gedik, Nat. Commun. **12**, 4837 (2021).
16. K. Kitagawa and H. Matsueda, J. Phys. Soc. Jpn. **91**, 104705 (2022).
17. T. Feldmaier, P. Strobel, M. Schmid, P. Hansmann, and M. Daghofer, Phys. Rev. Res. **2**, 033201 (2020).
18. J. Kanamori, Prog. Theor. Phys. **30**, 275 (1963).
19. J. Hubbard, Proc. R. Soc. A **277** (1369), 237 (1964).
20. R. O. Zaitsev, Sov. Phys. JETP **43**, 574 (1976).
21. K. A. Chao, J. Spalek, and A. M. Oles, J. Phys. C **10**, L271 (1977).
22. V. A. Gavrichkov, S. I. Polukeev, and S. G. Ovchinnikov, Phys. Rev. B **95**, 144424 (2017).
23. V. V. Val'kov and S. G. Ovchinnikov, Theor. Math. Phys. **50**, 466 (1982).
24. S. V. Vonsovskii and M. S. Svirskii, Sov. Phys. JETP **20**, 914 (1965).
25. V. M. Agranovich and B. S. Toshich, Sov. Phys. JETP **26**, 104 (1968).
26. M. J. R. Hoch, S. Nellutla, J. van Tol, E. S. Choi, J. Lu, H. Zheng, and J. F. Mitchell, Phys. Rev. B **79**, 214421 (2009).
27. K. Sato, A. Matsuo, K. Kindo, Y. Kobayashi, and K. Asai, J. Phys. Soc. Jpn. **78**, 093702 (2009).
28. A. Ikeda, T. Nomura, Y. H. Matsuda, A. Matsuo, K. Kindo, and K. Sato, Phys. Rev. B **93**, 220401(R) (2016).
29. V. Platonov, Y. B. Kudasov, M. Monakhov, and O. Tatsenko, Phys. Solid State **54**, 279 (2012).
30. M. M. Altarawneh, G.-W. Chern, N. Harrison, C. D. Batista, A. Uchida, M. Jaime, D. G. Rickel, S. A. Crooker, C. H. Mielke, J. B. Betts, J. F. Mitchell, and M. J. R. Hoch, Phys. Rev. Lett. **109**, 037201 (2012).
31. M. Rotter, Z.-S. Wang, A. T. Boothroyd, D. Prabhakaran, A. Tanaka, and M. Doerr, Sci. Rep. **4**, 7003 (2014).
32. A. Ikeda, S. Lee, T. T. Terashima, Y. H. Matsuda, M. Tokunaga, and T. Naito, Phys. Rev. B **94**, 115129 (2016).

Translated by R. Tyapaev